atmosphere

MDPI

Article

Airborne Prokaryotic, Fungal and Eukaryotic Communities of an Urban Environment in the UK

Hokyung Song [1,2], Nicholas Marsden [1], Jonathan R. Lloyd [1,*], Clare H. Robinson [1], Christopher Boothman [1], Ian Crawford [1], Martin Gallagher [1,*], Hugh Coe [1], Grant Allen [1] and Michael Flynn [1]

[1] Department of Earth and Environmental Sciences, The University of Manchester, Manchester M13 9PL, UK; hk.song15@jejunu.ac.kr (H.S.); nicholas.marsden@manchester.ac.uk (N.M.); clare.robinson@manchester.ac.uk (C.H.R.); christopher.boothman@manchester.ac.uk (C.B.); i.crawford@manchester.ac.uk (I.C.); hugh.coe@manchester.ac.uk (H.C.); grant.allen@manchester.ac.uk (G.A.); michael.flynn@manchester.ac.uk (M.F.)

[2] Subtropical/Tropical Organism Gene Bank, Jeju National University, 102 Jejudaehak-ro, Jeju 63243, Korea

* Correspondence: jon.lloyd@manchester.ac.uk (J.R.L.); martin.gallagher@manchester.ac.uk (M.G.)

Abstract: Bioaerosols often contain human pathogens and allergens affecting public health. However, relatively little attention has been given to bioaerosols compared with non-biological aerosols. In this study, we aimed to identify bioaerosol compositions in Manchester, UK by applying high throughput sequencing methods and to find potential sources. Samples were collected at Manchester Air Quality Super Site at the Firs Environmental Research Station in November 2019 and in February 2020. Total DNA has been extracted and sequenced targeting the 16S rRNA gene of prokaryotes, ITS region of fungal DNA and 18S rRNA gene of eukaryotes. We found marine environment-associated bacteria and archaea were relatively more abundant in the February 2020 samples compared with the November 2019 samples, consistent with the North West marine origin based on wind back-trajectory analysis. In contrast, an OTU belonging to *Methylobacterium*, which includes many species resistant to heavy metals, was relatively more abundant in November 2019 when there were higher metal concentrations. Fungal taxa that fruit all year were relatively more abundant in the February 2020 samples while autumn fruiting species generally had higher relative abundance in the November 2019 samples. There were higher relative abundances of land plants and algae in the February 2020 samples based on 18S rRNA gene sequencing. One of the OTUs belonging to the coniferous yew genus *Taxus* was more abundant in the February 2020 samples agreeing with the usual pollen season of yews in the UK which is from mid-January until late April. The result from this study suggests a potential application of bioaerosol profiling for tracing the source of atmospheric particles.

Keywords: bioaerosol; microbial community; high throughput sequencing; urban; UK

Citation: Song, H.; Marsden, N.; Lloyd, J.R.; Robinson, C.H.; Boothman, C.; Crawford, I.; Gallagher, M.; Coe, H.; Allen, G.; Flynn, M. Airborne Prokaryotic, Fungal and Eukaryotic Communities of an Urban Environment in the UK. *Atmosphere* **2022**, *13*, 1212. https://doi.org/10.3390/atmos13081212

Academic Editor: Salvatore Romano

Received: 23 April 2022
Accepted: 26 July 2022
Published: 1 August 2022

1. Introduction

Bioaerosols are a mixture of virus, bacteria, fungal spores and mycelium, plant pollens and debris of these components [1]. Traditionally, bioaerosols have been studied by culturing bacteria or by observing morphological characteristics of fungal spores or plant pollens under the microscope [2]. Over approximately the last decade, real-time detection methods have emerged which utilize various methods, ranging from holography to autofluorescence spectroscopy to identify and quantify bioaerosols [3–5]. Generally, these methods provide excellent time resolution, with 5 min sample integrations being typical, however, accurate speciation remains a significant technical challenge [6].

High throughput sequencing of 16S rRNA gene has been applied to identify microbial communities in diverse environments including soil [7–9], sediment [10,11], freshwater [12–14] and sea water [15,16]. To identify fungal species, primers targeting the intergenic spacer (ITS) region of DNA has been developed [17] and has been widely used [18,19]. For overall eukaryotic community analysis, the 18S rRNA gene is most commonly used [20,21]. As

sequencing has become cheaper and more widely available, there has been an increase in the number of studies in atmospheric sciences which incorporate the metabarcoding methods for bioaerosol identification [22,23]. Smith et al. [24] identified bacterial communities in the samples collected in the Earth's stratosphere based on 16S rRNA gene sequencing. Kraaijeveld et al. [25] used an Ion Torrent platform and supported the application of high throughput DNA sequencing for efficient and accurate monitoring of plant pollens in the atmosphere. Banchi et al. [26] applied metabarcoding techniques to identify fungal spores and observed fungal community composition in the air at higher resolution compared with using traditional microscopic approaches.

Although there has been an increase in the number of studies on bioaerosols in recent years, the source and transport of bioaerosols have been relatively less studied [27]. One of the few examples is Smith et al.'s study [28], which collected samples before, during, and after an Asian long range transport plume and found distinctive plume-associated bacterial and archaeal communities, suggesting intercontinental dispersal of these organisms by transpacific winds. Another example is Mu et al.'s study [29], which identified potential sources of airborne bacteria by applying Source Tracker [30] and revealed leaf surface as the main source both in mountainous and urban areas in Xi'an.

Manchester is one of the worst cities in the UK for poor air quality having over an annual mortality of over a hundred due to toxic air [31]. In the UK, by law, carbon monoxide (CO), nitrogen dioxide (NO_2), PM_{10} particulate matter, sulphur dioxide (SO_2), lead, benzene, and ozone (O_3) levels are being monitored to assess air quality. Bioaerosols, however, gained relatively less attention, although the impact of bioaerosols on public health and ecosystem functioning could be significant [1,32]. The present study aimed to identify airborne prokaryotic (bacteria and archaea), fungal, and eukaryotic community structure through high throughput sequencing and track potential sources of the bioaerosols in the Manchester Air Quality Supersite (MAQS) where the bioaerosol sampling system is co-located with an extensive suite of air quality sensors and instrumentation to monitor urban air quality.

2. Materials and Methods

2.1. Sample Collection

Filter samples were collected at the Manchester Air Quality Super Site at the Firs Environmental Research Station (53°27′ N, 2°13′ W) in Manchester, UK (http://www.cas.manchester.ac.uk/restools/firs/, accessed on 28 January 2022). Manchester is the second-most populous urban area in the UK, but also includes many green spaces (e.g., local parks). The sample collection site is approximately 4 km away from the city center. Samples were collected in two different time periods: (1) November 2019 and (2) February 2020 (Table 1). Filter samples were collected using an automatic high-volume aerosol sampler DHA-80 (DIGITEL Elektronik AG, Switzerland) [33,34]. During sampling, filters were automatically changed in every 24 h and collected at the end of each period. The air flow-rate of the sampler was ~500 L/min. Glass microfiber filters MG 227/1/60 with a diameter of 150 mm (Sartorius, Göttingen, Germany) were used to collect bioaerosol samples. The filters and filter holders were autoclaved before use. The inlet of the sampler was cleaned with a 1% Rely+On™ Virkon solution (LANXESS, Cologne, Germany) prior to collecting samples. Un-aspirated handling filters were also collected to assess potential contamination. Filters were transported to the laboratory at the University of Manchester and cut into 32 pieces per sample with sterile scissors. All of the samples collected in November 2019 were kept in a freezer for DNA extraction. Four out of thirty-two pieces of the samples collected in February 2020 were kept in a fridge for environmental scanning electronic microscopy (ESEM) and the rest were kept in a freezer for DNA extraction.

Table 1. Sample information.

Sample ID	Start Time	End Time
FIRS1_7	12 November 2019 13:16	13 November 2019 13:15
FIRS1_8	13 November 2019 13:16	14 November 2019 13:15
FIRS1_9	14 November 2019 13:16	15 November 2019 10:40
FIRS1_12	15 November 2019 10:40	16 November 2019 10:40
FIRS1_13	16 November 2019 10:40	17 November 2019 10:40
FIRS1_14	17 November 2019 10:40	18 November 2019 10:20
FIRS2_2	20 February 2020 16:25	21 February 2020 16:25
FIRS2_3	21 February 2020 16:25	22 February 2020 16:25
FIRS2_4	22 February 2020 16:25	23 February 2020 16:25
FIRS2_5	23 February 2020 16:25	24 February 2020 16:25
FIRS2_6	24 February 2020 16:25	25 February 2020 16:25
FIRS2_7	25 February 2020 16:25	26 February 2020 16:25
FIRS2_8	26 February 2020 16:25	27 February 2020 16:25

2.2. Assessment of Environmental Factors

Wind speed, direction, temperature, and humidity were measured at the supersite meteorological station which included a WindMaster sonic anemometer (Gill Instruments, Lymington, UK), with a time resolution of 20 Hz. Total precipitation rate was monitored using a Laser Precipitation Monitor (Theis, Göttingen, Germany). Particulate matter (PM_1, $PM_{2.5}$, PM_{10}, PMtotal) was measured with a Fidas 200 (Palas, Karlsruhe, Germany). CH_4 and CO_2 concentrations were obtained using a Multi-gas Carbon Emissions Analyzer (LGR, San Jose, CA, USA). CO concentration was obtained using a 48i CO Analyzer (Thermo Fisher, Waltham, MA, USA). NH_3 concentrations were obtained with an Economical Ammonia Analyzer (LGR, San Jose, CA, USA). Elemental composition was obtained with an Xact® 625i Multi-Metals Monitoring System (Cooper Environmental Services, Beaverton, OR, USA). More details on the air quality supersite and instruments can be found in Barker et al. [35].

2.3. Environmental Scanning Electronic Microscopy

Environmental Scanning Electron Microscopy (ESEM) was used to image the filter samples in backscattered electron (BSE) modes. Imaging was performed using a FEI Quanta 650 FEG ESEM operating at 15 kV under low-vacuum conditions (0.1–1.3 mbar). Energy dispersive spectroscopy (EDS) was performed using the Bruker ESPRIT software for element analysis.

2.4. DNA Extraction, PCR, and Sequencing

Sample DNA was extracted from the filters using the DNeasy PowerWater Kit (Qiagen) as described by the suppliers with an empty filter as an extraction control. The V4 region of 16S rRNA gene was amplified using the primers, 515F (5′-GTGYCAGCMGCCGCGGTAA-3′) and 806R (5′-GGACTACHVGGGTWTCTAAT-3′). PCR (polymerase chain reaction) condition for amplifying 16S rRNA gene was as follows: initial denaturation step at 95 °C for 2 min, 36 cycles of melting (95 °C, 30 s), annealing (58 °C, 30 s), and extension (72 °C, 2 min), and final extension at 72 °C for 5 min. The ITS (internal transcribed spacer) region of fungal DNA was amplified using the primers, ITS4-Fun (5′-AGCCTCCGCTTATTGATATGCTTAART-3′) and 5.8SR-Fun (5′-AACTTTYRRCAAYGGAT CWCT-3′). The PCR condition for amplifying fungal DNA was as follows: initial denaturation step at 95 °C for 30 s, 36 cycles of melting (95 °C, 30 s), annealing (56 °C, 45 s), and extension (72 °C, 2 min), and final extension at 72 °C for 5 min. The V9 region of the eukaryotic 18S rRNA gene was amplified using the primers, 1391F (5′-GTACACACCGCCCGTC-3′) and EukBr (5′-TGATCCT TCTGCAGGTTCACCTAC-3′). The PCR condition for amplifying eukaryotic 18S rRNA gene was as follows: initial denaturation step at 95 °C for 2 min, 37 cycles of melting (95 °C, 30 s), annealing (57 °C, 60 s), and extension (72 °C, 1.5 min), and final extension at 72 °C for 5 min.

Amplified DNAs were paired-end sequenced based on the Illumina MiSeq platform. The 18S rRNA gene amplicon sequencing of "FIRS2_4", "FIRS2_7", and "FIRS2_8" samples failed due to the low quantity of DNA. The raw fastq formatted sequence files were archived in the NCBI SRA (sequence read archive) under project number of PRJNA731031.

2.5. Sequence Analysis

Paired-end sequences were combined using the PANDASeq software v. 2. 8 [36]. Further sequence analysis including sequence alignment, quality control (e.g., removal of ambiguous sequences and chimeric sequences), classification, and OTU (operational taxonomic unit) clustering was performed using Mothur software v. 1. 42. 3 [37] following the MiSeq SOP (https://mothur.org/wiki/miseq_sop/, accessed on 2 July 2020). To remove chimeric sequences, VSEARCH v. 2. 13. 3 [38] was used. The Silva database v. 132 [39] was used for alignment and classification of sequences. OTUs were defined based on 97% sequence similarity using the OptiClust algorithm [40]. Singleton sequences, reads with sequences that are present only once in the dataset, were removed and OTUs with more than 100 reads in the extraction control were also removed. Since the Silva database provides taxonomic information only down to genus level, we used local BLASTn [41] software v. 2.9. 0 with the representative sequence of each OTUs against the NCBI nucleotide (nt) database [42] with e-value cutoff of 10^{-10}.

2.6. Quantitative PCR

Quantitative PCR (qPCR) was performed to obtain the absolute copy numbers of 16S rRNA and 18S rRNA genes. A dilution series of Telluria mixa DSM 4832 gBlock double stranded DNA gene fragment (Integrated DNA Technologies, Leuven, Belgium) was used to construct the standard curve for the qPCR reaction of the 16S rRNA genes. Saccharomyces cerevisiae NRRL Y-12632 gBlock double stranded DNA gene fragment (Integrated DNA Technologies, Leuven, Belgium) was used as a standard for qPCR of 18S rRNA genes. PCR amplification was performed in 25-µL reaction mixtures by using the Brilliant II SYBR green PCR master mix (Agilent Technologies, Santa Clara, CA, USA) 8F (5′AGAGTTTGATCCTGGCTCAG-3′) and 519R (5′-GWATTACCGCGGCKGCTG-3′) primers were used to quantify 16S rRNA genes and 1391F (5′-GTACACACCGCCCGTC-3′) and EukBr (5′-TGATCCTTCTGCAGGTTCACCTAC-3′) primers were used to quantify 18S rRNA genes. The PCR conditions for the amplification of 16S rRNA genes were as follows: initial denaturation step at 94 °C for 4 min, 36 cycles of melting (94 °C, 30 s), annealing (50 °C, 15 s), and extension (72 °C, 45 s). The PCR conditions for the amplification of 18S rRNA genes was as follows: initial denaturation step at 94 °C for 4 min, 36 cycles of melting (94 °C, 30 s), annealing (55 °C, 30 s), and extension (72 °C, 1 min). Triplicate of the DNA samples were amplified and monitored with the Rotor Gene Q instrument (Qiagen, Hilden, Germany). Cycle threshold (CT) was determined automatically by the instrument.

2.7. Statistical Analysis

Prior to diversity analysis, samples were sub-sampled into 108,230 reads per sample for prokaryotes, 4637 reads per sample for eukaryotes, and 53,056 reads per sample for fungi. To compare environmental conditions between the two sampling periods, to compare the relative abundance of taxonomic groups between the two sampling periods and to compare diversity between the two sampling periods, *t*-test was performed. When the assumptions for the *t*-test could not be met, a Wilcoxon rank sum test was performed instead. The number of reads were square-root transformed and the Bray–Curtis dissimilarity was calculated to draw principal coordinates analysis (PCoA) plots. To fit environmental variables onto the PCoA ordinations, the 'envfit' function in R 'vegan' package [43] was used. To test the significance of community distances between sampling time, an analysis of similarity (ANOSIM) test was performed. nMDS plot visualization and ANOSIM test was performed using the PRIMER 6 software [44].

3. Results

3.1. Environmental Parameters

Table S1 shows the average value of environmental parameters during each of the sample collection. The average temperature ranged from 5.4–7.8 °C when collecting November 2019 samples and 3.6–9.3 °C when collecting February 2020 samples (Table S1). The average humidity was over 80% in both of the sampling periods. The total precipitation rate was higher when collecting February 2020 samples (Table S2, Figure 1). Concentrations of heavy metals, for example, Ti, Mn, Fe, Cu, Zn, As, Zr, Nb, Pd, Te, Pb, and Bi, were significantly higher in the samples collected in November 2019 compared with those from February 2020 (Figure 1). In contrast, Cl concentrations were higher in the February 2020 samples.

Figures 2 and 3 shows a series of 96-h Lagrangian back trajectories for airmasses arriving over the sampling site at an altitude of 400 m, calculated using the HYSPLIT (The Hybrid Single Particle Lagrangian Integrated Trajectory) modeling system with full 3D advection [45]. HYSPLIT was driven using GFS (Global Forecast System) 0.25-degree gridded meteorological reanalysis data. A 400 m receptor altitude was chosen to represent a layer consistent with the well-mixed planetary boundary layer at the measurement site (and high enough to prevent model particles colliding with the ground). The trajectories illustrate North-West marine-derived winds when collecting February 2020 samples and mostly land/continental origin of winds during November 2019 sampling. Environmental scanning electronic microscopy showed attachment of a C-containing feature (10 μm length, possibly a fungal spore) with NaCl in one of the February 2020 samples (Figure S5). This corresponds to the back trajectory of the winds coming from the North-West marine environment (Figure 3).

During November 2019, the particulate mass was generally below DEFRA (Department for Environment, Food and Rural Affairs) air quality limit values (Figure S1), however, some significant exceedances were observed, e.g., 03/11 and 06/11, where $PM_{2.5}$ and PM_{10} exceed the DEFRA limits of 20 μg m^{-3} and 40 μg m^{-3}, respectively; $PM_{2.5}$ excided these limits during filter collection on the 16th and 17th of November. Fewer exceedances were observed during February 2020 (Figure S2), and none occurred during the filter sampling period. Figures S3 and S4 show polar concentration plots as a function of wind speed and direction for the two sampling periods, where the greatest aerosol loadings are typically observed at low wind speeds, suggesting local sources are important at the site. Significant enhancements in PM_{10} as compared with PM_1 and $PM_{2.5}$ were observed at higher wind speeds, and this was particularly prevalent during the February sampling period; the November period demonstrated an enhancement in PM_{10} from the South West which was not present in the PM_1 loading, suggesting that there may be a separate and distinct source of large aerosol from this wind sector.

3.2. Prokaryotic Community Structure and Diversity

There was no significant difference in the absolute copy number of 16S rRNA genes between the November 2019 samples and February 2020 samples based on the qPCR results (Figure S6). The most abundant phylum on average was Proteobacteria, followed by Bacteroidota, Actinobacteria and Firmicutes (Figure 4a). The relative abundance of Bacteroidota was significantly higher in the November 2019 samples compared with the February 2020 samples, whereas the relative abundances of Verrucomicrobiota, Cyanobacteria, Planctomycetota, Acidobacteriota, and Chloroflexi were higher in the February 2020 samples (Table S3). The most abundant genus was *Hymenobacter* during both of the sampling periods. The second most abundant genus was *Methylobacterium-Methylorubrum* in November 2019 samples and *Flavobacterium* in February 2020 samples (Figure 4b).

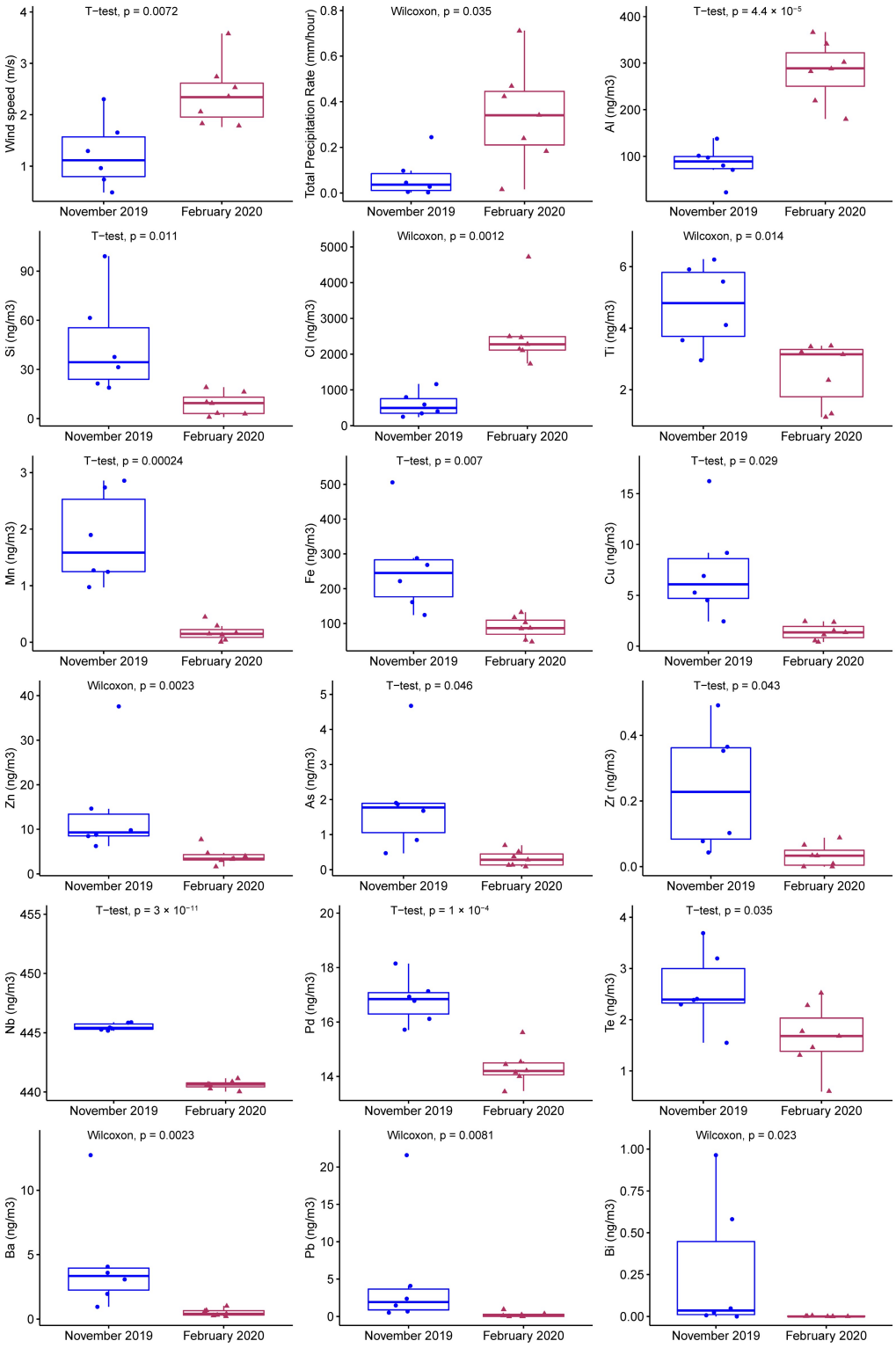

Figure 1. Boxplots of environmental parameters that were significantly different between November 2019 samples and February 2020 samples.

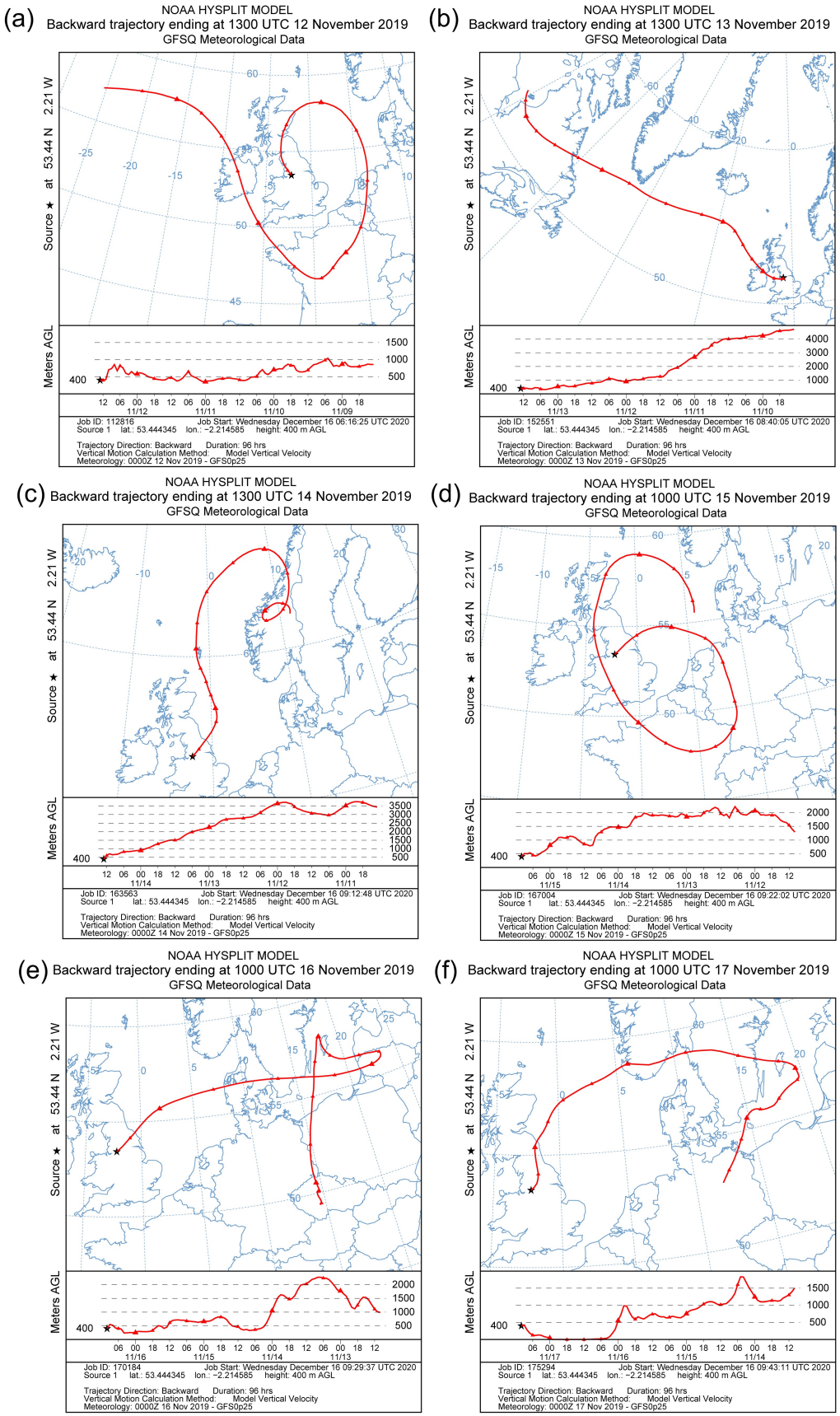

Figure 2. 96 h HYSPLIT Lagrangian back trajectories of air at the start point of each sample collected in November 2019. (**a**) "FIRS1_7", (**b**) "FIRS1_8", (**c**) "FIRS1_9", (**d**) "FIRS1_12", (**e**) "FIRS1_13" and (**f**) "FIRS1_14".

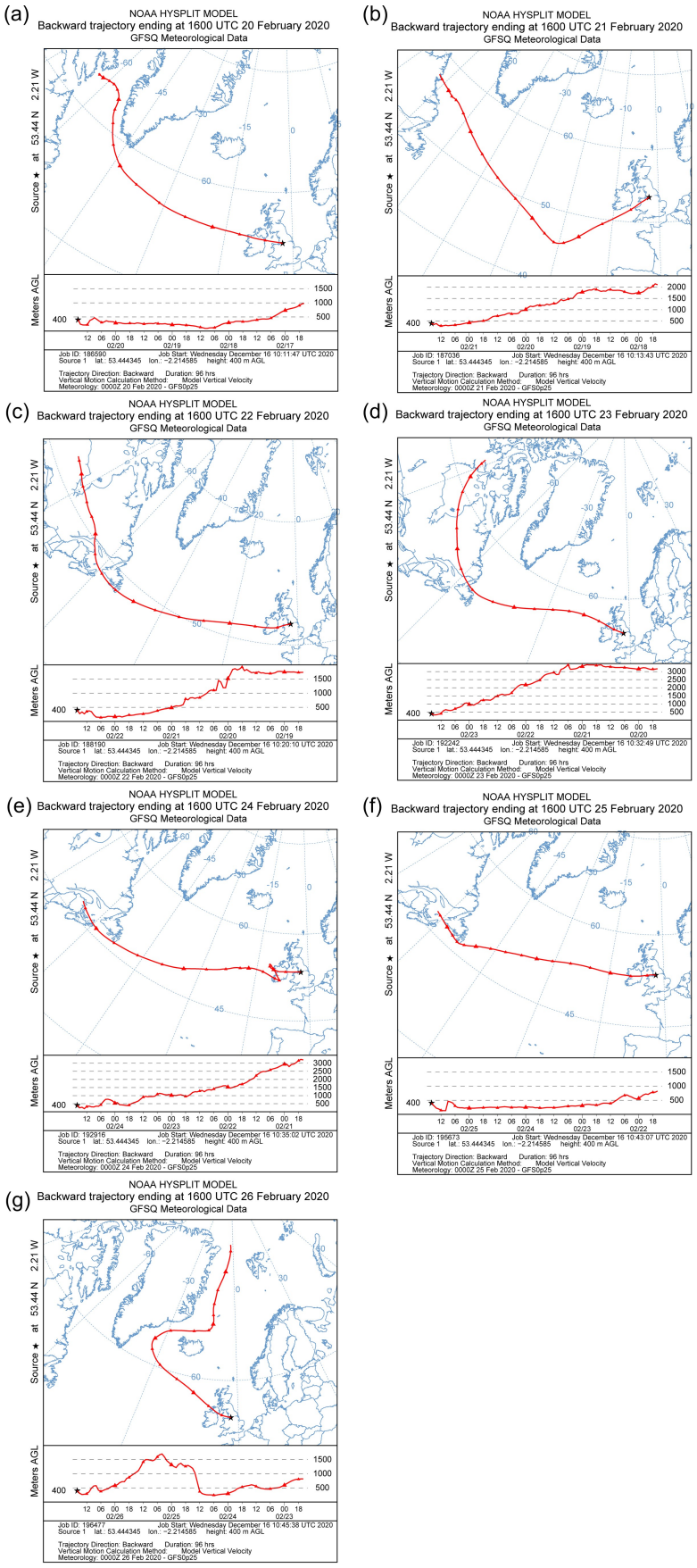

Figure 3. 96 h HYSPLIT Lagrangian back trajectories of air at the start point of each sample collected in February 2020. (**a**) "FIRS2_2", (**b**) "FIRS2_3", (**c**) "FIRS2_4", (**d**) "FIRS2_5", (**e**) "FIRS2_6", (**f**) "FIRS2_7" and (**g**) "FIRS2_8".

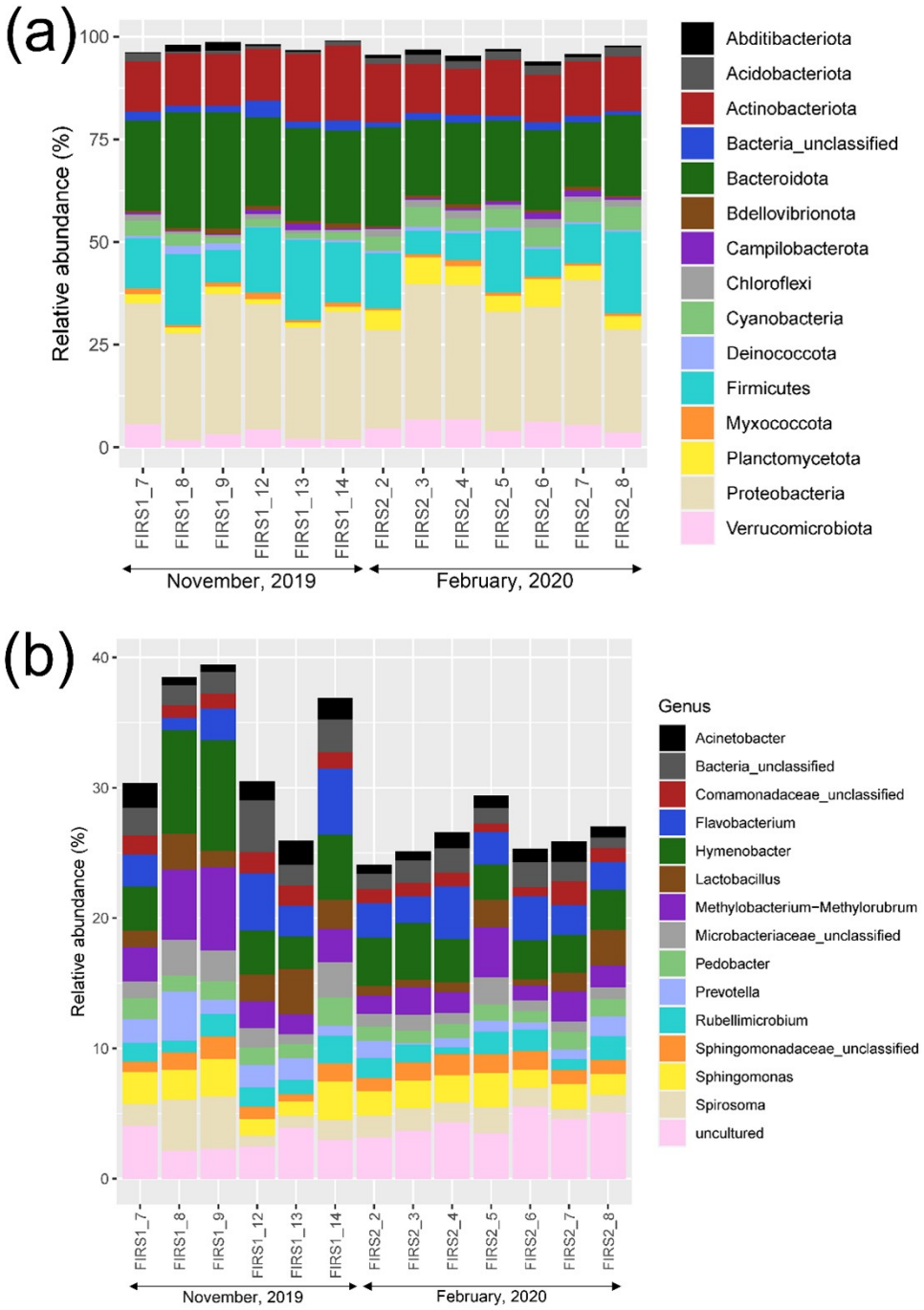

Figure 4. The 15 most abundant prokaryotic phyla (**a**) and genera (**b**) in the samples.

Table 2 shows *t*-test (or Wilcoxon test) results of the 30 most abundant OTUs revealing significant differences in their relative abundance between the November 2019 samples and the February 2020 samples. The average relative abundance of OTU00020 was about six times higher in the November 2019 samples and had 100% similarity with *Methylobacterium bullatum* and *Methylobacterium marchantiae* based on blast search against the NCBI 16S rRNA sequence database. OTUs that had higher relative abundance in the February 2020 samples included marine environment associated taxa. For example, OTU000087, which was the most abundant archaeal OTU in the samples collected, was affiliated with "Marine Group II" based on the Silva database and had no blast matches with >80% similarity against the NCBI nt database. OTU000115, which was also relatively more abundant in the February 2020 samples, was affiliated with "SAR86_clade" based on the Silva database and had no

blast match with > 90% similarity. OTU000147, which was affiliated with "Marinimicrobia ge" based on the Silva database and had no blast match with > 81% similarity, was also more abundant in the February 2020 samples.

Figure 5 shows a PCoA plot generated based on the Bray–Curtis distance of prokaryotic communities between the samples. There was a significant difference in prokaryotic community composition during the two different sampling periods based on the ANOSIM test (global R of 0.606 and *p*-value of 0.001). Environmental factors that were significantly correlated with the ordination are added as red arrows. Cl, Al, and wind speed were pointing towards the February 2020 samples, whereas Si, Pd, Nb, Mn, Fe, Cu, and Zr were pointing towards the November 2019 samples, confirming their significant association with the prokaryotic communities during each sampling period. In terms of alpha diversity, Shannon diversity values were significantly higher in the samples collected in February 2020 in comparison with November 2019 samples (Figure S7). However, there was no difference in the number of OTUs between the two sample sets.

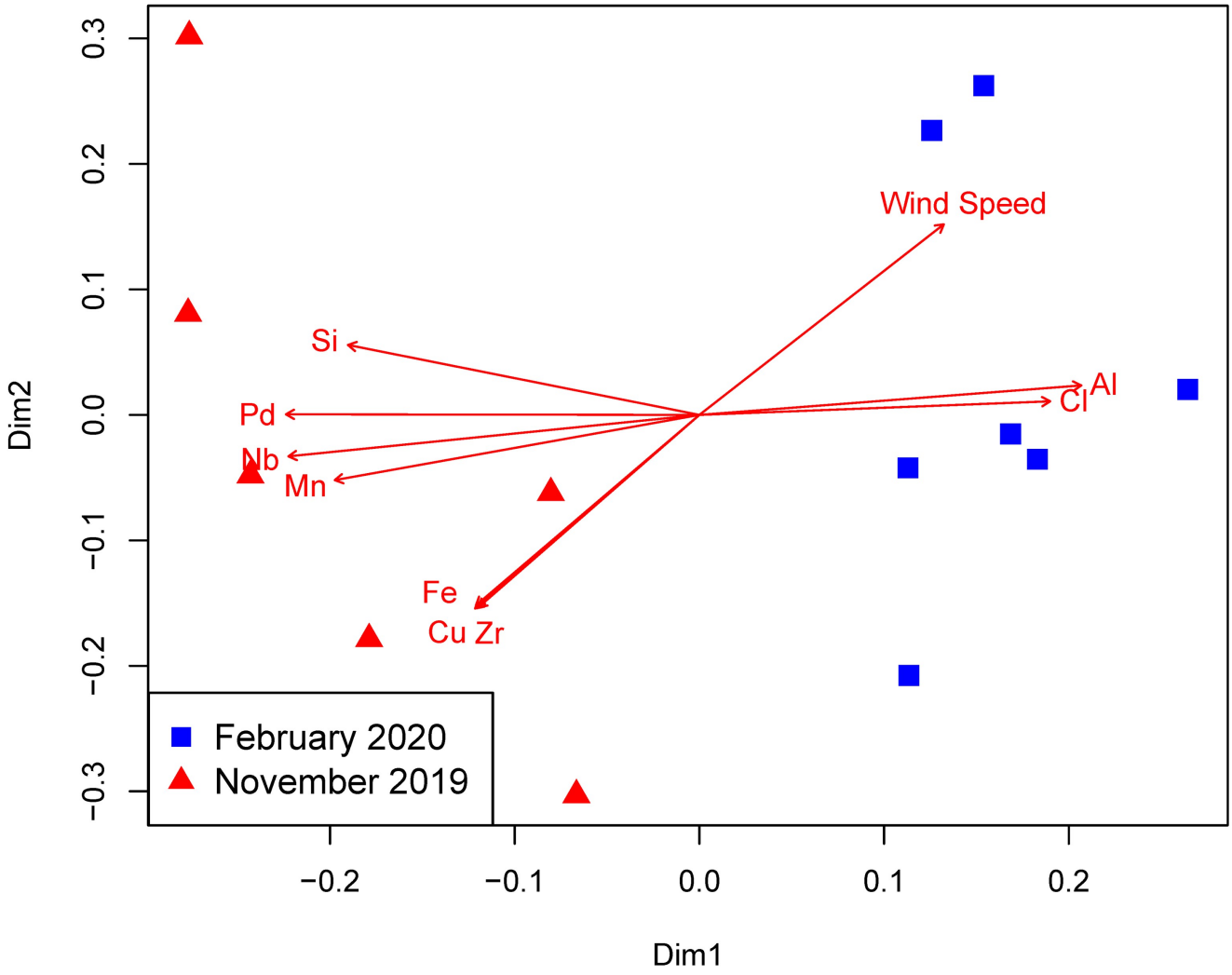

Figure 5. PCoA (principal coordinate analysis) plot of prokaryotic communities. Environmental factors that have significant correlation with the ordination (with p value lower than 0.01 and R-square value larger than 0.5) based on permutation tests are shown as red arrows.

Table 2. *t*-test (or Wilcoxon test) results of the 30 most abundant prokaryotic OTUs that show significant difference in their relative abundance between the November 2019 samples and the February 2020 samples. Their taxonomic annotation based on the Silva database and their BLAST result against NCBI nt database (best hit score, classified down to species level) are shown together.

OTU ID	*p* Value	Nov_2019 Average (%)	Feb_2020 Average (%)	Taxonomy Based on the Silva Database	BLAST against NCBI nt Database		
					Taxonomy	Similarity (%)	E-Value
Otu000020	0.045	1.136	0.187	*Methylobacterium-Methylorubrum*	*Methylobacterium bullatum, Methylobacterium marchantiae*	100	6×10^{-120}
Otu000014	0.017	0.762	0.470	*Rubellimicrobium*	*Rubellimicrobium aerolatum*	100	9×10^{-112}
Otu000019	0.032	0.648	0.433	*Pedobacter*	*Pedobacter miscanthi, Pedobacter helvus*, and etc.	100	2×10^{-125}
Otu000048	0.016	0.654	0.046	Bacteria_unclassified	*Calycina alstrupii*	88.29	9×10^{-73}
Otu000047	0.012	0.406	0.201	*Streptococcus*	*Streptococcus gallolyticus, Streptococcus pasteurianus*, and etc.	100	8×10^{-125}
Otu000054	0.018	0.604	0.021	Moraxellaceae_ge	*Agitococcus lubricus*	97.62	3×10^{-117}
Otu000058	0.020	0.367	0.161	*Lactobacillus*	*Lactobacillus johnsonii, Lactobacillus paragasseri*, and etc.	100	2×10^{-125}
Otu000053	0.037	0.097	0.345	*Rickettsiella*	*Diplorickettsia massiliensis* 20B	98.02	3×10^{-118}
Otu000099	0.036	0.331	0.076	*Prevotella*	*Prevotella hominis*	99.6	1×10^{-123}
Otu000089	0.018	0.371	0.039	*Spirosoma*	*Spirosoma oryzae*	96.83	2×10^{-114}
Otu000102	0.003	0.283	0.103	*Aureimonas*	*Aureimonas glaciei*	100	2×10^{-125}
Otu000122	0.036	0.296	0.062	*Pseudomonas*	*Paucimonas lemoignei, Pseudomonas versuta*, and etc.	100	2×10^{-125}
Otu000090	0.005	0.051	0.270	uncultured	*Roseimicrobium gellanilyticum*	87.3	6×10^{-82}
Otu000120	0.023	0.315	0.041	Staphylococcaceae_unclassified	*Mammaliicoccus fleurettii, Mammaliicoccus sciuri*, and etc.	100	2×10^{-125}
Otu000108	0.030	0.212	0.115	*Dyadobacter*	*Dyadobacter frigoris, Dyadobacter hamtensis*	99.6	1×10^{-123}
Otu000129	0.041	0.238	0.090	*Chryseobacterium*	*Chryseobacterium solani, Epilithonimonas ginsengisoli*, and etc.	100	2×10^{-125}
Otu000111	0.038	0.206	0.115	*Corynebacterium*	*Corynebacterium freneyi, Corynebacterium xerosis*	100	7×10^{-126}
Otu000091	0.037	0.063	0.215	*Pseudarcobacter*	*Arcobacter suis, Arcobacter caeni*	100	2×10^{-125}
Otu000087	0.002	0.000	0.251	Marine_Group_II_ge	*Methanobrevibacter cuticularis*	79.45	3×10^{-54}
Otu000148	0.013	0.174	0.080	*Spirosoma*	*Spirosoma pomorum*	96.83	2×10^{-114}
Otu000115	0.011	0.023	0.208	SAR86_clade_ge	*Pseudomonas nabeulensis*	89.33	8×10^{-87}
Otu000143	0.003	0.014	0.194	Corynebacteriales_unclassified	*Rhodococcus aerolatus*	100	2×10^{-125}
Otu000202	0.010	0.201	0.032	Comamonadaceae_unclassified	*Xylophilus rhododendri, Ramlibacter rhizophilus*, and etc.	100	2×10^{-125}
Otu000141	0.001	0.033	0.173	*Sphingomonas*	*Sphingomonas flava*	99.6	1×10^{-123}
Otu000147	0.033	0.037	0.155	Marinimicrobia__ge	*Acinetobacter piscicola, Acinetobacter marinus*	80.57	2×10^{-57}
Otu000162	0.043	0.024	0.164	*Scytonema_UTEX_2349*	*Hassallia antarctica*	99.6	1×10^{-123}
Otu000246	0.025	0.169	0.035	1174-901-12	*Lichenihabitans psoromatis, Beijerinckia mobilis*	95.63	4×10^{-110}
Otu000183	0.004	0.003	0.164	Crocinitomicaceae_unclassified	*Wandonia haliotis*	95.63	4×10^{-110}
Otu000230	0.016	0.005	0.155	Cyanobacteriia_unclassified	*Lobosphaera incisa*	87.7	5×10^{-83}
Otu000206	0.035	0.023	0.136	*Calothrix_PCC-6303*	*Macrochaete lichenoides*	99.21	1×10^{-122}

3.3. Fungal Community Structure and Diversity

The most abundant phylum on average was Basidiomycota followed by Ascomycota (Figure 6a). The relative abundance of Basidiomycota was significantly higher in the November 2019 samples compared with the February 2020 samples, whereas the relative abundance of Ascomycota was higher in the February 2020 samples (Table S4). The most abundant genus in the November 2019 samples was *Mycena*, followed by *Clitocybe* and *Phlebia*, whereas the most abundant genus in the February 2020 samples was *Daedaleopsis*, followed by *Xylodon* and *Piptoporus* (Figure 6b).

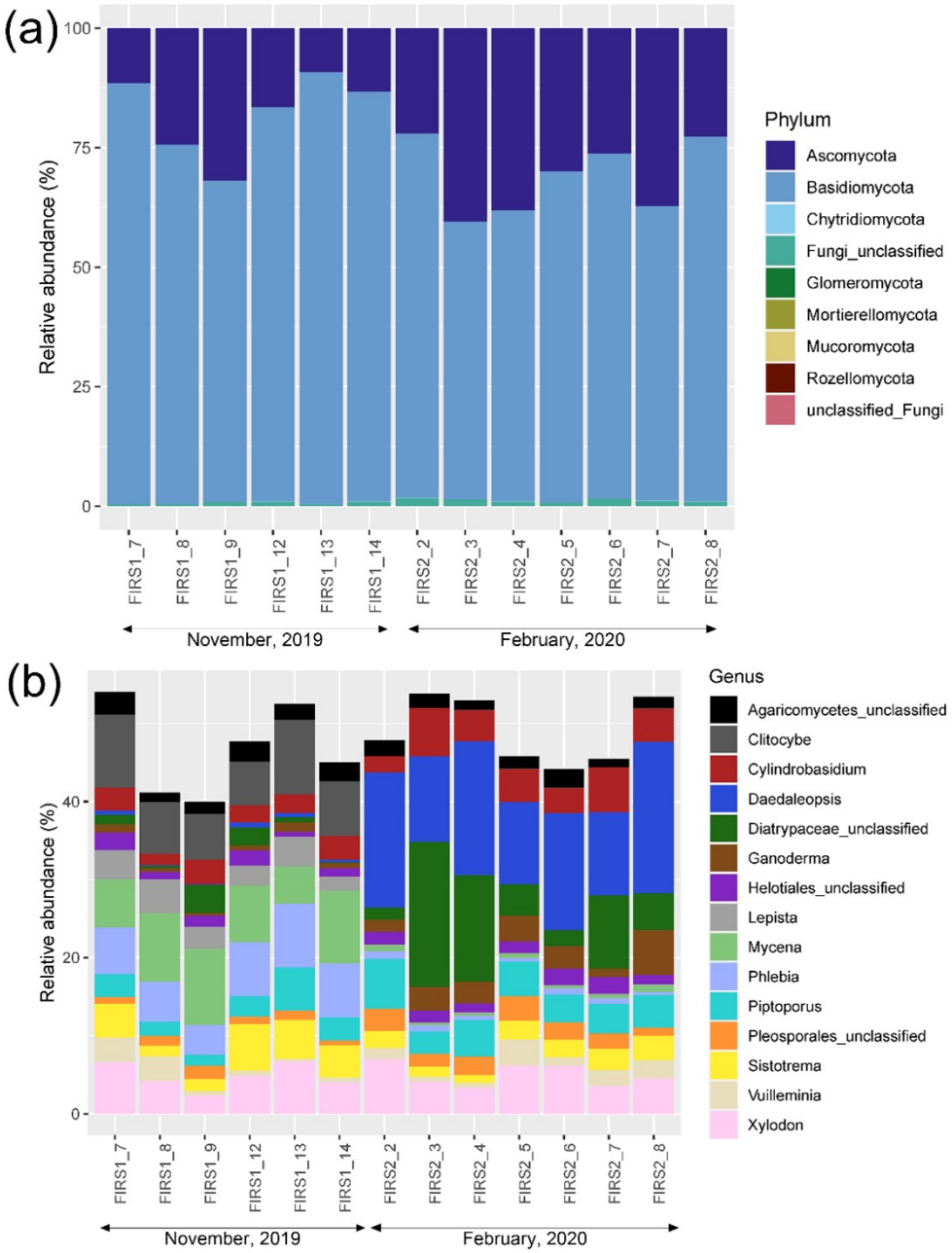

Figure 6. The 15 most abundant fungal phyla (**a**) and genera (**b**) in the samples.

Table 3 shows the *t*-test (or Wilcoxon test) results of the 30 most abundant fungal OTUs that shows significant difference in their relative abundance between the November 2019 samples and the February 2020 samples. The relative abundance of fungal OTUs during the two different sampling time matched with their fruiting season (Supplementary Information). The OTUs annotated with fungal taxa that fruit all year round, for exam-

ple, OTU000003 (*Daedaleopsis confragosa*) and Otu000009 (*Cylindrobasdium evolvens*), had generally higher relative abundance in the February 2020 samples, while the OTUs annotated with fungal taxa that fruit in autumn, for example, Otu000006 (*Clitocybe nebularis*), Otu000016 (*Lepista_nuda)* and Otu000026 (*Paralepista flaccida*), had generally higher relative abundance in the November 2019 samples.

Figure 7 shows a PCoA plot generated based on the Bray–Curtis distance of fungal communities between samples. There was a significant difference between the samples collected in November 2019 and the samples collected in February 2020 based on the ANOSIM test (global R of 1 and *p*-value of 0.002). Environmental factors that have significant correlation with the ordination are added as red arrows. Cl, Al, and wind speed arrows were pointing towards the February 2020 samples whereas Nb, Mn, Pd, Si, Fe, Cu, Zr, and CH_4 were pointing towards the November 2019 samples. Shannon diversity and the number of fungal OTUs were significantly higher in the samples collected in November 2019 in comparison with February 2020 samples (Supplementary Figure S8).

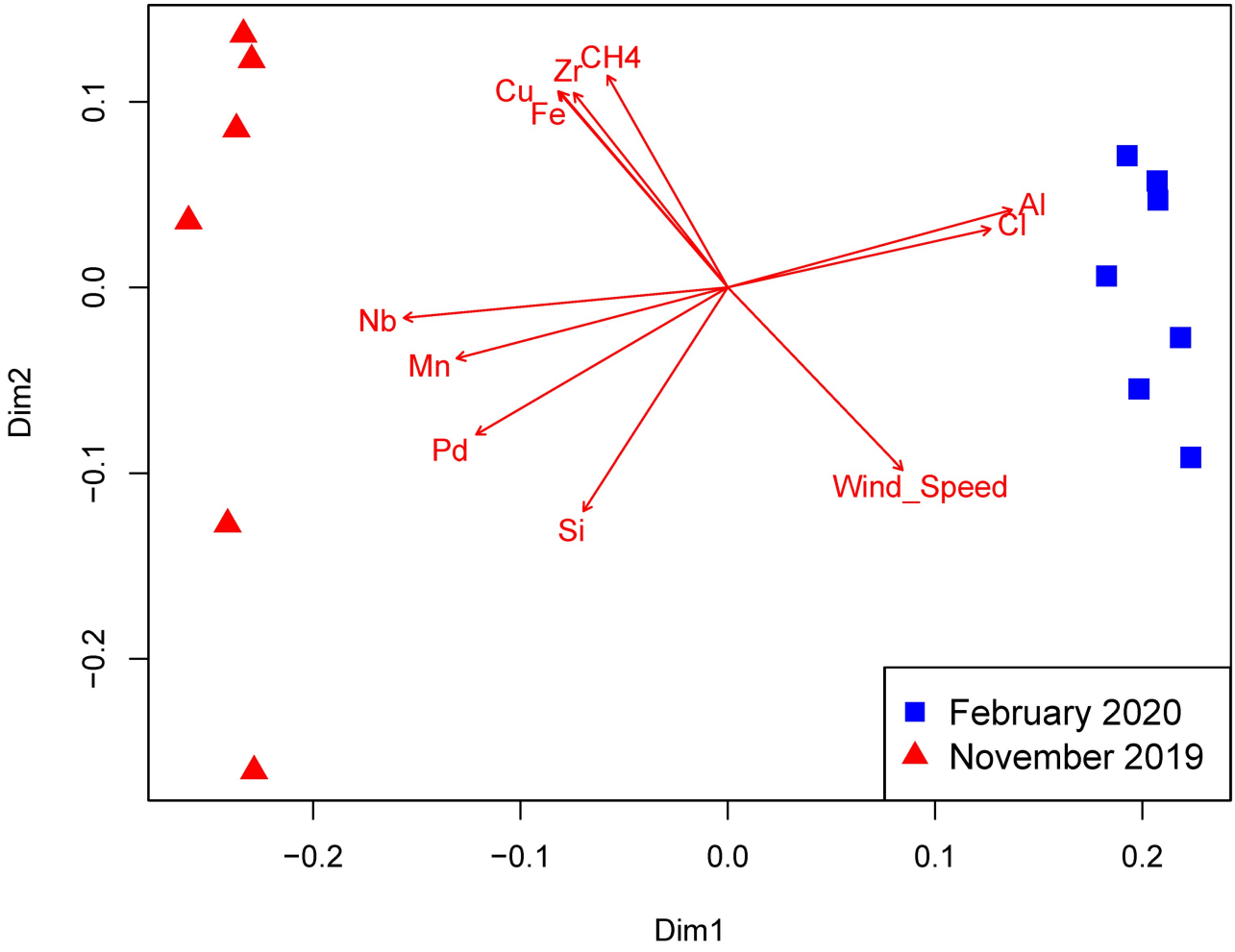

Figure 7. PCoA (principal coordinate analysis) plot of fungal communities. Environmental factors that have significant correlation with the ordination (with p value lower than 0.01 and R-square value larger than 0.5) based on permutation tests are shown as red arrows.

Table 3. *t*-test (or Wilcoxon test) results of the 30 most abundant fungal OTUs that shows significant difference in their relative abundance between the November 2019 samples and the February 2020 samples. Their taxonomic annotation based on the UNITE database and their BLAST result against NCBI nt database (best hit score, classified down to species level) are shown together.

OTU ID	*p* Value	Nov_2019 Average (%)	Feb_2020 Average (%)	Taxonomy Based on the UNITE Database	BLAST against NCBI nt Database		
					Taxonomy	Similarity (%)	E-Value
Otu000003	0.000	0.405	14.467	Daedaleopsis_unclassified	*Daedaleopsis confragosa*, *Lenzites betulinus*, and etc.	100	0
Otu000004	0.000	6.017	0.522	Phlebia_unclassified	*Phlebia radiata*	100	0
Otu000006	0.002	6.225	0.001	*Clitocybe_nebularis*	*Leucopaxillus tricolor*, *Lepista nebularis*	100	0
Otu000009	0.018	2.468	4.198	*Cylindrobasidium_evolvens*	*Polyporus gayanus*	99.567	0
Otu000010	0.003	4.192	0.006	*Mycena_metata*	*Mycena arcangeliana*	98.966	0
Otu000013	0.029	2.621	0.600	*Sistotrema_oblongisporum*	*Clavulina cristata*	83.252	2.91×10^{-95}
Otu000016	0.001	2.451	0.036	*Lepista_nuda*	*Lepista nuda*	99.208	0
Otu000017	0.006	0.609	2.896	*Ganoderma_australe*	*Ganoderma australe*	99.728	0
Otu000022	0.001	1.635	0.000	*Infundibulicybe_geotropa*	*Ampulloclitocybe clavipes*	94.01	8.94×10^{-160}
Otu000023	0.017	1.503	0.061	Peniophora_unclassified	*Peniophora piceae*	96.961	2.34×10^{-170}
Otu000026	0.001	1.510	0.000	*Paralepista_flaccida*	*Paralepista gilva*	99.73	0
Otu000029	0.007	1.164	0.325	*Radulomyces_molaris*	*Cuphophyllus colemannianus*	90.517	1.63×10^{-77}
Otu000031	0.035	0.487	0.268	*Coprinellus_micaceus*	*Coprinellus micaceus*, *Coprinus rufopruinatus*	100	0
Otu000034	0.001	0.364	1.184	Heterobasidion_unclassified	*Podoscypha multizonata*, *Podoscypha involuta*	100	0
Otu000035	0.001	0.764	0.101	*Hypholoma_fasciculare*	*Hypholoma fasciculare*	100	0
Otu000037	0.034	1.030	0.088	*Trechispora_byssinella*	*Trechispora byssinella*	99.189	0
Otu000040	0.033	0.440	1.002	*Antrodia_xantha*	*Amyloporia xantha*, *Antrodia xantha*	100	0
Otu000042	0.001	0.200	1.328	Polyporaceae_unclassified	*Trametes gibbosa*	100	0
Otu000043	0.001	0.058	1.506	Diatrypaceae_unclassified	*Eutypa lata*	100	9.68×10^{-169}
Otu000044	0.041	0.514	0.776	Russulales_unclassified	*Peniophora incarnata*	100	0
Otu000045	0.000	0.990	0.034	Clitocybe_unclassified	*Clitocybe vibecina*	99.733	0
Otu000046	0.017	0.454	0.856	Xenasmatella_unclassified	*Phlebiella borealis*	98.864	1.74×10^{-176}
Otu000048	0.006	0.069	1.288	Xylariales_unclassified	*Eutypa lata*	100	2.70×10^{-169}
Otu000049	0.012	0.442	0.716	*Hyphodontia_pallidula*	*Hyphodontia pallidula*	99.446	0
Otu000050	0.001	0.193	1.048	Pleosporales_unclassified	*Phaeosphaeria caricicola*	94.375	7.65×10^{-135}
Otu000051	0.001	0.886	0.000	*Rhodocollybia_butyracea*	*Rhodocollybia butyracea*	99.542	0
Otu000052	0.002	0.270	0.885	*Resinicium_bicolor*	*Resinicium bicolor*	100	0
Otu000054	0.003	0.202	0.665	*Flammulina_velutipes*	*Flammulina velutipes*	100	0
Otu000056	0.001	0.587	0.105	*Pleurotus_ostreatus*	*Pleurotus sapidus*, *Pleurotus ostreatus*, and etc.	100	0
Otu000058	0.027	0.606	0.042	Hyaloscyphaceae_unclassified	*Lachnum virgineum*	93.631	3.52×10^{-128}

3.4. Eukaryotic Community Structure and Diversity

There was no significant difference in the absolute copy number of 16S rRNA genes between the November 2019 samples and February 2020 samples based on the qPCR results (Figure S9). Figure 8a shows the phylum level composition of eukaryotic communities classified based on the 18S rRNA gene in each of the sample. The most abundant phylum was Basidiomycota in the samples collected in November 2019. However, in contrast, the most abundant phylum in the samples collected in February 2020 was Phragmoplastophyta, which includes algae and land plants. The *t*-test (or Wilcoxon test) results showed that the relative abundance of Basidiomycota was significantly higher in the November 2019 samples compared with the February 2020 samples, whereas the relative abundances of Phragmoplastophyta and Diatomea were higher in the February 2020 samples (Table S5). Most of the sequences were unclassified at genus level (Figure 8b) based on the Silva database.

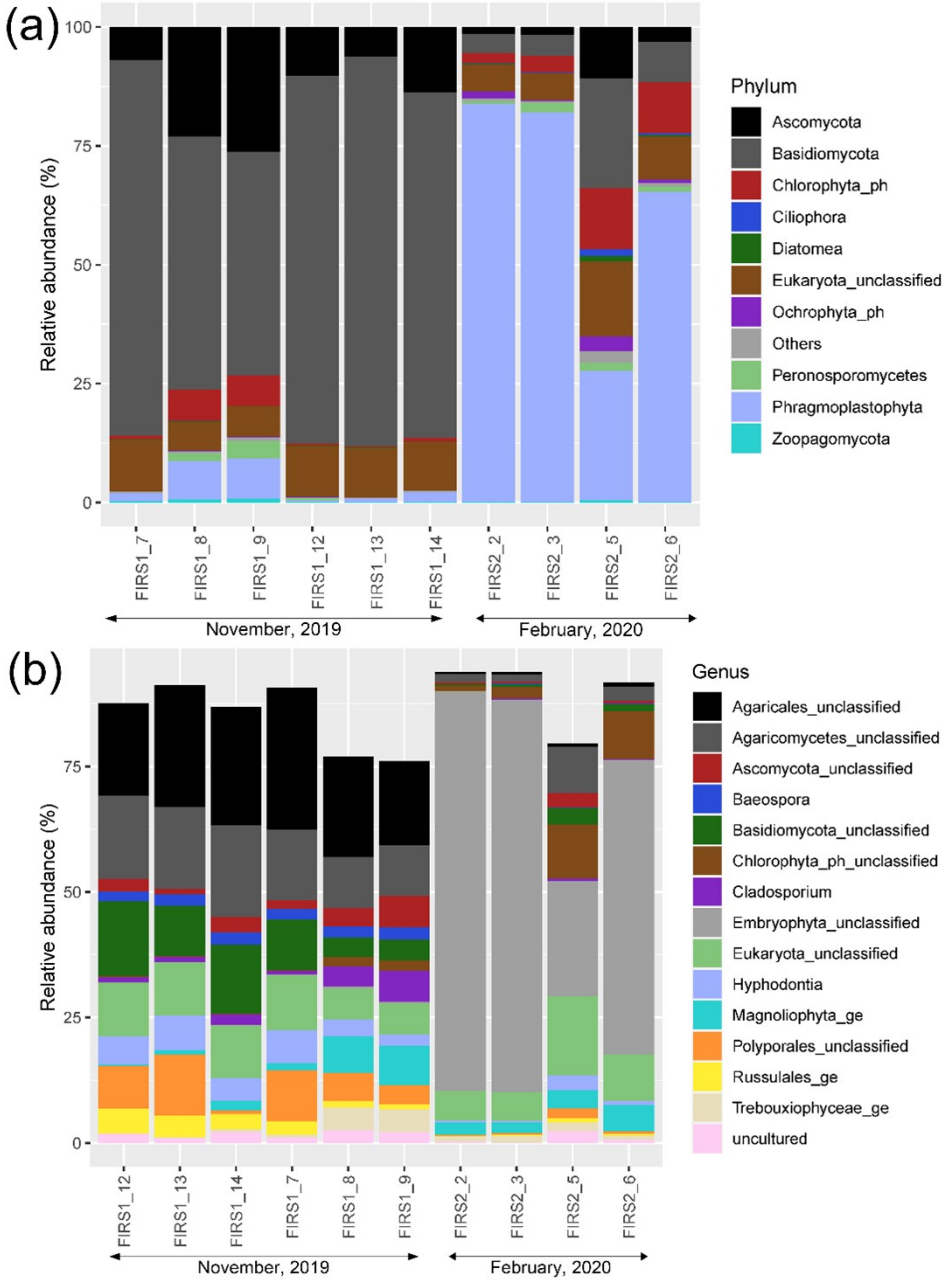

Figure 8. The 15 most abundant eukaryotic phyla (**a**) and genera (**b**) in the samples.

Table 4 shows the *t*-test (or Wilcoxon test) results of the 30 most abundant eukaryotic OTUs that show significant difference in their relative abundance between the November 2019 samples and the February 2020 samples. We found OTUs belonging to *Taxus* (Otu00011, Otu00136, Otu00258) of which pollens are common in the UK from mid-January until late April peaking in late February until mid-March (according to the pollen calendar produces by National Pollen and Aerobiology Research Unit, University of Worcester in 2012) to be relatively more abundant in the February 2020 samples. Otu00001, which had 100% similarity with species belonging to *Lepista* was relatively more abundant in the November 2019 samples than the February 2020 samples which corresponds with the ITS sequence data (Table 3). Otu00029 was classified as Chlorophyta and was relatively more abundant in the February 2020 samples compared with the November 2019 samples.

Figure 9 shows a PCoA plot generated based on the Bray–Curtis distance of eukaryotic communities between samples. There was a significant difference between the samples collected in November 2019 and the samples collected in February 2020 based on the ANOSIM test (global R of 0.996 and *p*-value of 0.005). Environmental factors that have significant correlation with the ordination are added as red arrows. Cl and Al arrows were pointing towards the February 2020 samples whereas Nb was pointing towards the November 2019 samples. There was no significant difference in Shannon diversity and in the number of fungal OTUs between the samples collected in November 2019 and in February 2020 (Figure S10).

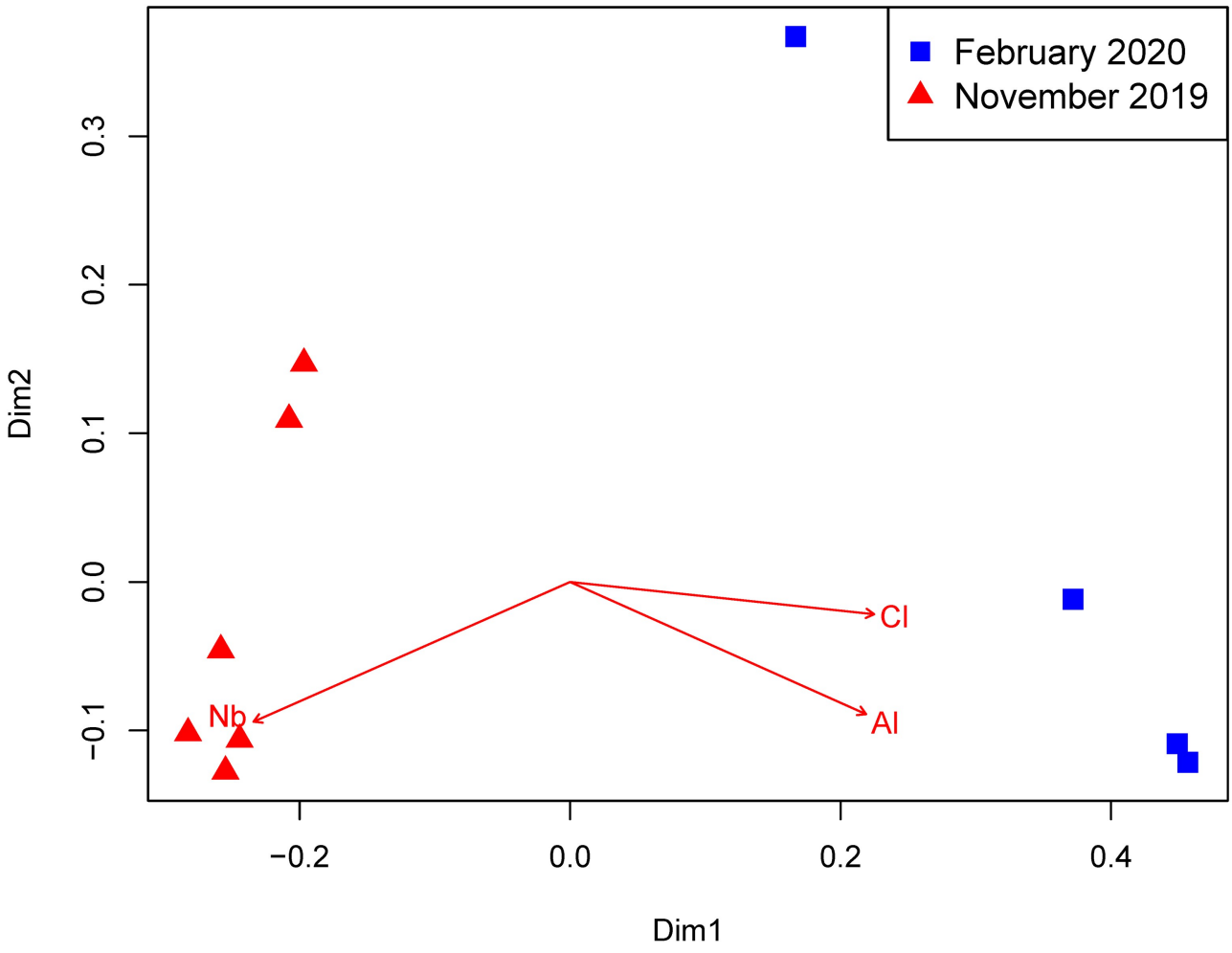

Figure 9. PCoA (principal coordinate analysis) plot of eukaryotic communities. Environmental factors that have significant correlation with the ordination (with p value lower than 0.01 and R-square value larger than 0.5) based on permutation tests are shown as red arrows.

Table 4. *t*-test (or Wilcoxon test) results of the 30 most abundant eukaryotic OTUs that shows significant difference in their relative abundance between the November 2019 samples and the February 2020 samples. Their taxonomic annotation based on the Silva database and their BLAST result against NCBI nt database (best hit score, classified down to species level) are shown together.

OTU ID	*p* Value	Nov_2019 Average (%)	Feb_2020 Average (%)	Taxonomy Based on the Silva Database	BLAST against NCBI nt Database		
					Taxonomy	Similarity (%)	E-Value
Otu00011	0.006	0.000	56.006	Embryophyta_unclassified	*Taxus wallichiana*	100	3.06×10^{-49}
Otu00001	0.000	17.691	0.270	Agaricales_unclassified	*Lepista sordida*, *Lepista saeva*, etc.	100	1.09×10^{-48}
Otu00002	0.014	6.563	0.323	Polyporales_unclassified	*Fomitopsis pinicola*, *Antrodia albida*, etc.	100	1.09×10^{-48}
Otu00003	0.013	5.611	0.749	Basidiomycota_unclassified	*Sistotrema brinkmannii*, *Sistotrema oblongisporum*	100	1.09×10^{-48}
Otu00004	0.008	4.137	1.057	*Hyphodontia*	*Hyphodontia rimosissima*	95.413	2.37×10^{-40}
Otu00029	0.038	0.708	5.812	Chlorophyta_ph_unclassified	*Trebouxia impressa*	100	1.09×10^{-48}
Otu00006	0.002	3.249	0.092	Agaricomycetes_unclassified	*Phlebia radiata*	100	1.09×10^{-48}
Otu00008	0.011	2.879	0.377	Russulales_ge	*Peniophora nuda*	98.165	1.82×10^{-46}
Otu00012	0.000	2.193	0.038	*Baeospora*	*Baeospora myosura*	100	1.09×10^{-48}
Otu00015	0.014	2.013	0.275	Agaricomycetes_unclassified	*Rogersella griseliniae*	95.413	2.37×10^{-40}
Otu00016	0.011	2.077	0.000	Magnoliophyta_ge	*Parietaria judaica*	100	8.61×10^{-50}
Otu00017	0.023	1.714	0.367	Eukaryota_unclassified	*Sterigmatomyces halophilu*	90.991	5.16×10^{-32}
Otu00136	0.006	0.000	2.890	Eukaryota_unclassified	*Taxus wallichiana*	99.09	1.00×10^{-45}
Otu00024	0.013	1.218	0.005	Basidiomycota_unclassified	*Chamaeota sinica*	93.578	5.12×10^{-37}
Otu00028	0.038	0.942	0.199	Eukaryota_unclassified	*Hyphodontia crustosa*	92.661	2.38×10^{-35}
Otu00035	0.025	0.744	0.248	Agaricomycetes_unclassified	*Burgoa anomala*, *Sistotrema octosporum*, etc.	100	1.09×10^{-48}
Otu00031	0.002	0.726	0.162	Agaricomycetes_unclassified	*Rogersella griseliniae*	91.818	1.11×10^{-33}
Otu00032	0.013	0.802	0.005	Agaricales_unclassified	*Mycena galericulata*	98.165	2.35×10^{-45}
Otu00258	0.006	0.000	1.068	Embryophyta_unclassified	*Taxus wallichiana*	99.09	1.00×10^{-45}
Otu00039	0.000	0.665	0.022	Agaricomycetes_unclassified	*Mycena galericulata*	95.413	2.37×10^{-40}
Otu00041	0.042	0.550	0.102	*Hyphodontia*	*Hyphodontia nespori*	100	1.09×10^{-48}
Otu00036	0.013	0.600	0.005	Sporidiobolaceae_unclassified	*Sporobolomyces carnicolor*, *Sporobolomyces patagonicus*, etc.	100	1.09×10^{-48}
Otu00040	0.024	0.571	0.027	Eukaryota_unclassified	*Tulasnella violea*	97.222	3.88×10^{-43}
Otu00049	0.011	0.528	0.075	*Trechispora*	*Trechispora alnicola*	93.578	5.12×10^{-37}
Otu00043	0.011	0.536	0.000	Agaricales_unclassified	*Chrysomphalina grossula*	96.33	5.08×10^{-42}
Otu00057	0.011	0.503	0.000	Pleosporales_unclassified	*Cochliobolus kusanoi*, *Epicoccum nigrum*	100	1.09×10^{-48}
Otu00051	0.008	0.453	0.070	Agaricales_unclassified	*Chondrostereum purpureum*	100	8.45×10^{-45}
Otu00063	0.022	0.439	0.049	Sordariomycetes_unclassified	*Lopadostoma polynesium*, *Monographella lycopodina*, etc.	100	1.09×10^{-48}
Otu00054	0.039	0.385	0.124	Eukaryota_unclassified	*Jaculispora submersa*	98.165	2.35×10^{-45}
Otu00060	0.023	0.403	0.049	Eukaryota_unclassified	*Repetobasidium conicum*	92.661	2.38×10^{-35}

4. Discussion

In this study, we used high throughput sequencing to monitor bioaerosols in Manchester, which is the second most populated city in the UK. The air quality based on $PM_{2.5}$ and PM_{10} levels during sampling periods were in general under the limit. However, there were some days in November 2019 when $PM_{2.5}$ level was over the air quality limit. The heavy metal concentrations were also higher in November 2019 sampling period. Regarding bioaerosol composition, the relative abundance of potential pathogens, for example, OTUs belonging to *Methylobacterium*, *Streptococcus* and *Corynebacterium* were higher in the November 2019 samples. Species belonging to *Methylobacterium* are known to be opportunistic pathogens which cause bacteremia in immunocompromised people [46,47]. Many species belonging to *Streptococcus* are pathogenic to humans, causing bacteremia, sepsis, pneumonia, and other diseases [48]. *Corynebacterium* include pathogenic bacterial species which cause a wide range of serious infections including diphtheria [49]. Considering these facts, the air quality in November 2019 seemed to be generally worse than February 2020, both in terms of non-bioaerosol and bioaerosol compositions.

The 5-year average data (Weather Spark, https://weatherspark.com/, accessed on 2 July 2022) show similar weather conditions in November and February in Manchester. During our sampling periods, the temperatures in November and February were similar, but wind directions, wind speeds and precipitation rates were different. In November 2019, the winds mostly originated from land/continent and the wind speed was slower than February 2020. In addition, the precipitation rate was lower than February 2020 sampling period. Considering these weather conditions, the air particles originating from anthropogenic activities (with high metal concentrations) seemed to persist for a long time during this sampling period. The higher relative abundance of the OTU belonging to *Methylobacterium* in November 2019 samples could also be linked with higher heavy metal concentrations as many of the species belonging to *Methylobacterium* are known to be heavy metal resistant [50,51].

During February 2020 sampling, Cl concentration was high which could be associated with the marine sourced winds. Agreeing with this, the relative abundance of marine environment-related taxa was higher in the February 2020 samples. For example, the relative abundance of Cyanobacteria and OTUs belonging to Marine Group II and SAR86 were higher in February 2020 samples. Species belonging to Cyanobacteria are mostly photosynthetic and are naturally found in various types of water environments. Marine Group II is a group of planktonic archaea predominantly found in ocean surface waters for which little genomic information is available and lacking cultured representatives [52]. SAR86 is one of the most abundant uncultured assemblages of bacteria found in ocean surface water [53].

In our study, fungal (spores) and plant (pollen) compositions were well explained by seasonal difference. Basidiomycetes of which the relative abundance was higher in the November 2019 samples are associated with decaying deciduous and coniferous trees and liter. There was a prominent difference in the eukaryotic phylum composition during the two sampling periods where in November 2019, most (> 50% on average) of the sequences were annotated as Basidiomycota whereas in February 2020, most (> 50% on average) of the sequences were annotated as Phragmoplastophyta. This corresponds with the results from Sharma Ghimire et al.'s study [54] which showed fungal loadings being highest in autumn and lowest in winter in an urban city in China.

There were some overlaps in the abundant phylum and genera found in our study with other urban and suburban areas. We found Proteobacteria, Bacteroidota, Actinobacteria and Firmicutes being the most dominant phyla. In Núñez et al.'s [55] study, Actinobacteria and Proteobacteria were dominant in the air of Madrid, Spain. Stewart et al. [23] studied airborne bacterial communities in Philadelphia, USA and found Proteobacteria to be the most dominant phylum. They also found Proteobacteria, Firmicutes, Actinobacteria and Bacteroidetes to be relatively more abundant in the urban area whereas Cyanobacteria, Tenericutes, Fusobacteria, and Deionococcus were more abundant in suburban area.

Hymenobacteria, which was the most abundant genera in our samples, was also one of the dominant genera in a rapidly developing city in China [56]. A high abundance of *Methylobacterium* was observed in an suburban site in Toyama City, Japan [57].

The fungal compositions we found in this study were also to some extent similar to other urban studies. For example, in Sharma Ghimire et al.'s study [54], *Clitocybe* was one of the dominant fungal genera where it was abundant in spring and autumn and almost absent in summer and winter. In our study, the OTU annotated as *Clitocybe nebularis* was more abundant in November 2019 samples than in February 2020 samples, which agrees with their study. Woo et al. [58] studied wet and dry deposition of fungi in Seoul, South Korea and found *Daedaleopsis* being more abundant in wet deposition. In our study, *Daedaleopsis* was more abundant in February 2020 samples when the precipitation rate was higher.

There was a large proportion of Embryophyta in the February samples, but most of them were unclassified at the lower taxonomic levels when classified based on the Silva database. The reason is that Silva database itself does not include reference genomes of Embryophyta down to lower taxonomic levels. There is a need for a well-curated database for 18S rRNAs with high resolutions and until then, NCBI nt database could work as a substitute.

5. Conclusions

In this study, we used high throughput sequencing to monitor airborne prokaryotic, fungal, and eukaryotic communities in Manchester, UK. In November 2019 when the winds were slowly blowing from continent/land with less precipitation, the air quality was generally worse both in terms of biological and non-biological aerosol compositions than in February 2020. We found significant changes in the urban bioaerosol composition due to seasonal variation combined with local and long-range sources. In November 2019 there was higher relative abundance of an OTU that belongs to *Methylobacterium* which corresponds with higher heavy metal concentrations. In contrast, in February 2020 when the winds were blowing from the North-West marine environment, bacterial, archaeal and algae taxa were found to be abundant in marine/water environment, for example, Cyanobacteria, Marine Group II, SAR86_clade and Chlorophyta were relatively more abundant. In terms of fungal and other eukaryotic communities, bioaerosol compositions corresponded with seasonal differences. We found Basidiomycetes, which includes many species of decaying deciduous and coniferous trees and litter, relatively more abundant in November 2019 samples whereas more of plant-originated sequences (mostly undefined based on Silva database) were found in February 2020 samples. As for 18S rRNA sequencing, there is a demand for a well-curated database with high resolution. Overall, the results from this study suggest a potential application of bioaerosol profiling for tracing the source of atmospheric particles and influencing factors in an urban environment.

Supplementary Materials: The following supporting information can be downloaded at: https://www.mdpi.com/article/10.3390/atmos13081212/s1, Figure S1: PM_1, $PM_{2.5}$ and PM_{10} aerosol mass during the November 2019 sampling period; Figure S2: PM_1, $PM_{2.5}$ and PM_{10} aerosol mass during the February 2020 sampling period; Figure S3: Polar plot of PM_1, $PM_{2.5}$ and PM_{10} aerosol mass loadings for the November 2019 sampling period. Polar plots are a function of wind speed and wind direction, with concentric rings representing 1 m s^{-1} increments; Figure S4: Polar plot of PM_1, $PM_{2.5}$ and PM_{10} aerosol mass loadings for the February 2020 sampling period. Polar plots are a function of wind speed and wind direction, with concentric rings representing 1 m s^{-1} increments; Figure S5: Environmental scanning electronic microscopy image showing attachment of NaCl to a C containing feature; Figure S6: 16S/18S rRNA gene copy number per m^3 of air in each sample; Figure S7: Shannon diversity and the number of prokaryotic OTUs found in the samples collected in November 2019 and in February 2020; Figure S8: Shannon diversity and the number of fungal OTUs found in the samples collected in November 2019 and in February 2020; Figure S9: 16S/18S rRNA gene copy number per m^3 of air in each sample; Figure S10: Shannon diversity and the number of eukaryotic OTUs found in the samples collected in November 2019 and in February 2020; Table S1:

Average value of each of the environmental parameter during sample collection; Table S2: *t*-test (or Wilcoxon rank sum test) results of environmental parameters compared between the two sampling periods; Table S3: *t*-test (or Wilcoxon rank sum test) result comparing the relative abundance of prokaryotic phylum between November 2019 samples and February 2020 samples; Table S4: *t*-test (or Wilcoxon rank sum test) result comparing the relative abundance of fungal phylum between November 2019 samples and February 2020 samples; Table S5: *t*-test (or Wilcoxon rank sum test) results comparing the relative abundance of eukaryotic phylum between November 2019 samples and February 2020 samples.

Author Contributions: Conceptualization, J.R.L., C.H.R., M.G. and G.A.; Methodology, N.M., M.G., I.C., C.B., H.C. and M.F.; Formal Analysis, H.S.; Investigation, N.M., I.C., C.B., H.S., M.G. and M.F.; Writing—Original Draft Preparation, H.S.; Writing—Review and Editing, C.H.R., I.C., J.R.L., M.G. and G.A.; Visualization, H.S.; Supervision, C.H.R., J.R.L. and M.G.; Project Administration, M.G.; Funding Acquisition, M.G. All authors have read and agreed to the published version of the manuscript.

Funding: The authors acknowledge the support of Natural Environment Research Council (NERC) via grant "Towards a UK Airborne Bioaerosol Climatology" (NE/S002049/1).

Data Availability Statement: The raw fastq formatted sequence files were archived in the NCBI SRA (sequence read archive) under project number of PRJNA731031.

Acknowledgments: Hokyung Song and Ian Crawford were funded by the NERC grant BIOARC, NE/S002049/1. The authors gratefully acknowledge the NOAA Air Resources Laboratory (ARL) for the provision of the HYSPLIT transport and dispersion model and READY website (https://www.ready.noaa.gov, assessed on 9 November 2020) used in this publication.

Conflicts of Interest: The authors declare no conflict of interest.

References

1. Fröhlich-Nowoisky, J.; Kampf, C.J.; Weber, B.; Huffman, J.A.; Pöhlker, C.; Andreae, M.O.; Lang-Yona, N.; Burrows, S.M.; Gunthe, S.S.; Elbert, W.; et al. Bioaerosols in the Earth system: Climate, health, and ecosystem interactions. *Atmos. Res.* **2016**, *182*, 346–376. [CrossRef]
2. Wittmaack, K.; Wehnes, H.; Heinzmann, U.; Agerer, R. An overview on bioaerosols viewed by scanning electron microscopy. *Sci. Total Environ.* **2005**, *346*, 244–255. [CrossRef] [PubMed]
3. Crouzy, B.; Stella, M.; Konzelmann, T.; Calpini, B.; Clot, B. All-Optical automatic pollen identification: Towards an operational system. *Atmos. Environ.* **2016**, *140*, 202–212. [CrossRef]
4. Šaulienė, I.; Šukienė, L.; Daunys, G.; Valiulis, G.; Vaitkevičius, L.; Matavulj, P.; Brdar, S.; Panic, M.; Sikoparija, B.; Clot, B.; et al. Automatic pollen recognition with the Rapid-E particle counter: The first-level procedure, experience and next steps. *Atmos. Meas. Tech.* **2019**, *12*, 3435–3452. [CrossRef]
5. Crawford, I.; Topping, D.; Gallagher, M.; Forde, E.; Lloyd, J.R.; Foot, V.; Stopford, C.; Kaye, P. Detection of Airborne Biological Particles in Indoor Air Using a Real-Time Advanced Morphological Parameter UV-LIF Spectrometer and Gradient Boosting Ensemble Decision Tree Classifiers. *Atmosphere* **2020**, *11*, 1039. [CrossRef]
6. Huffman, J.A.; Perring, A.E.; Savage, N.J.; Clot, B.; Crouzy, B.; Tummon, F.; Shoshanim, O.; Damit, B.; Schneider, J.; Sivaprakasam, V.; et al. Real-Time sensing of bioaerosols: Review and current perspectives. *Aerosol Sci. Technol.* **2020**, *54*, 465–495. [CrossRef]
7. Amoo, A.E.; Babalola, O.O.; Stewart, F.J. Microbial Diversity of Temperate Pine and Native Forest Soils Profiled by 16S rRNA Gene Amplicon Sequencing. *Microbiol. Resour. Announc.* **2021**, *10*, e00298-21. [CrossRef]
8. Jiang, H.; Chen, Y.; Hu, Y.; Wang, Z.; Lu, X. Soil Bacterial Communities and Diversity in Alpine Grasslands on the Tibetan Plateau Based on 16S rRNA Gene Sequencing. *Front. Ecol. Evol.* **2021**, *9*, 630722. [CrossRef]
9. Semenov, M.V. Metabarcoding and Metagenomics in Soil Ecology Research: Achievements, Challenges, and Prospects. *Biol. Bull. Rev.* **2021**, *11*, 40–53. [CrossRef]
10. Pearman, J.K.; Thomson-Laing, G.; Howarth, J.D.; Vandergoes, M.J.; Thompson, L.; Rees, A.; Wood, S.A. Investigating variability in microbial community composition in replicate environmental DNA samples down lake sediment cores. *PLoS ONE* **2021**, *16*, e0250783. [CrossRef]
11. Ghate, S.D.; Shastry, R.P.; Arun, A.B.; Rekha, P.D. Unraveling the bacterial community composition across aquatic sediments in the Southwestern coast of India by employing high-throughput 16S rRNA gene sequencing. *Reg. Stud. Mar. Sci.* **2021**, *46*, 101890. [CrossRef]
12. Zhu, C.; Zhang, J.; Nawaz, M.Z.; Mahboob, S.; Al-Ghanim, K.A.; Khan, I.A.; Lu, Z.; Chen, T. Seasonal succession and spatial distribution of bacterial community structure in a eutrophic freshwater Lake, Lake Taihu. *Sci. Total Environ.* **2019**, *669*, 29–40. [CrossRef]

13. Cavaco, M.A.; St. Louis, V.L.; Engel, K.; St. Pierre, K.A.; Schiff, S.L.; Stibal, M.; Neufeld, J.D. Freshwater microbial community diversity in a rapidly changing High Arctic watershed. *FEMS Microbiol. Ecol.* **2019**, *95*, fiz161. [CrossRef]
14. Malki, K.; Rosario, K.; Sawaya, N.A.; Székely, A.J.; Tisza, M.J.; Breitbart, M.; Moran, M.A. Prokaryotic and Viral Community Composition of Freshwater Springs in Florida, USA. *mBio* **2020**, *11*, e00436-20. [CrossRef]
15. Ul-Hasan, S.; Bowers, R.M.; Figueroa-Montiel, A.; Licea-Navarro, A.F.; Beman, J.M.; Woyke, T.; Nobile, C.J. Community ecology across bacteria, archaea and microbial eukaryotes in the sediment and seawater of coastal Puerto Nuevo, Baja California. *PLoS ONE* **2019**, *14*, e0212355. [CrossRef]
16. Wang, Y.; Liu, Y.; Wang, J.; Luo, T.; Zhang, R.; Sun, J.; Zheng, Q.; Jiao, N. Seasonal dynamics of bacterial communities in the surface seawater around subtropical Xiamen Island, China, as determined by 16S rRNA gene profiling. *Mar. Pollut. Bull.* **2019**, *142*, 135–144. [CrossRef]
17. Schoch, C.L.; Seifert, K.A.; Huhndorf, S.; Robert, V.; Spouge, J.L.; Levesque, C.A.; Chen, W.; Bolchacova, E.; Voigt, K.; Crous, P.W.; et al. Nuclear ribosomal internal transcribed spacer (ITS) region as a universal DNA barcode marker for fungi. *Proc. Natl. Acad. Sci. USA* **2012**, *109*, 6241–6246. [CrossRef]
18. Yuan, T.; Zhang, H.; Feng, Q.; Wu, X.; Zhang, Y.; McCarthy, A.J.; Sekar, R. Changes in Fungal Community Structure in Freshwater Canals across a Gradient of Urbanization. *Water* **2020**, *12*, 1917. [CrossRef]
19. Sommermann, L.; Geistlinger, J.; Wibberg, D.; Deubel, A.; Zwanzig, J.; Babin, D.; Schlüter, A.; Schellenberg, I. Fungal community profiles in agricultural soils of a long-term field trial under different tillage, fertilization and crop rotation conditions analyzed by high-throughput ITS-Amplicon sequencing. *PLoS ONE* **2018**, *13*, e0195345. [CrossRef]
20. Banerji, A.; Bagley, M.; Elk, M.; Pilgrim, E.; Martinson, J.; Santo Domingo, J. Spatial and temporal dynamics of a freshwater eukaryotic plankton community revealed via 18S rRNA gene metabarcoding. *Hydrobiologia* **2018**, *818*, 71–86. [CrossRef]
21. Müller, C.A.; de Mattos Pereira, L.; Lopes, C.; Cares, J.; dos Anjos Borges, L.G.; Giongo, A.; Graeff-Teixeira, C.; Loureiro Morassutti, A. Meiofaunal diversity in the Atlantic Forest soil: A quest for nematodes in a native reserve using eukaryotic metabarcoding analysis. *For. Ecol. Manag.* **2019**, *453*, 117591. [CrossRef]
22. Tanaka, D.; Sato, K.; Goto, M.; Fujiyoshi, S.; Maruyama, F.; Takato, S.; Shimada, T.; Sakatoku, A.; Aoki, K.; Nakamura, S. Airborne Microbial Communities at High-Altitude and Suburban Sites in Toyama, Japan Suggest a New Perspective for Bioprospecting. *Front. Bioeng. Biotechnol.* **2019**, *7*, 12. [CrossRef]
23. Stewart, J.D.; Shakya, K.M.; Bilinski, T.; Wilson, J.W.; Ravi, S.; Choi, C.S. Variation of near surface atmosphere microbial communities at an urban and a suburban site in Philadelphia, PA, USA. *Sci. Total Environ.* **2020**, *724*, 138353. [CrossRef]
24. Smith, D.J.; Ravichandar, J.D.; Jain, S.; Griffin, D.W.; Yu, H.; Tan, Q.; Thissen, J.; Lusby, T.; Nicoll, P.; Shedler, S.; et al. Airborne Bacteria in Earth's Lower Stratosphere Resemble Taxa Detected in the Troposphere: Results From a New NASA Aircraft Bioaerosol Collector (ABC). *Front. Microbiol.* **2018**, *9*, 1752. [CrossRef]
25. Kraaijeveld, K.; de Weger, L.A.; Ventayol García, M.; Buermans, H.; Frank, J.; Hiemstra, P.S.; den Dunnen, J.T. Efficient and sensitive identification and quantification of airborne pollen using next-generation DNA sequencing. *Mol. Ecol. Resour.* **2015**, *15*, 8–16. [CrossRef]
26. Banchi, E.; Ametrano, C.G.; Stanković, D.; Verardo, P.; Moretti, O.; Gabrielli, F.; Lazzarin, S.; Borney, M.F.; Tassan, F.; Tretiach, M.; et al. DNA metabarcoding uncovers fungal diversity of mixed airborne samples in Italy. *PLoS ONE* **2018**, *13*, e0194489. [CrossRef]
27. Xie, W.; Li, Y.; Bai, W.; Hou, J.; Ma, T.; Zeng, X.; Zhang, L.; An, T. The source and transport of bioaerosols in the air: A review. *Front. Environ. Sci. Eng.* **2020**, *15*, 44. [CrossRef]
28. Smith, D.J.; Timonen, H.J.; Jaffe, D.A.; Griffin, D.W.; Birmele, M.N.; Perry, K.D.; Ward, P.D.; Roberts, M.S. Intercontinental Dispersal of Bacteria and Archaea by Transpacific Winds. *Appl. Environ. Microbiol.* **2013**, *79*, 1134–1139. [CrossRef]
29. Mu, F.; Li, Y.; Lu, R.; Qi, Y.; Xie, W.; Bai, W. Source identification of airborne bacteria in the mountainous area and the urban areas. *Atmos. Res.* **2020**, *231*, 104676. [CrossRef]
30. Knights, D.; Kuczynski, J.; Charlson, E.S.; Zaneveld, J.; Mozer, M.C.; Collman, R.G.; Bushman, F.D.; Knight, R.; Kelley, S.T. Bayesian community-wide culture-independent microbial source tracking. *Nat. Methods* **2011**, *8*, 761–763. [CrossRef]
31. Taleghani, M. Air Pollution within Different Urban Forms in Manchester, UK. *Climate* **2022**, *10*, 26. [CrossRef]
32. Gollakota, A.R.K.; Gautam, S.; Santosh, M.; Sudan, H.A.; Gandhi, R.; Sam Jebadurai, V.; Shu, C.-M. Bioaerosols: Characterization, pathways, sampling strategies, and challenges to geo-environment and health. *Gondwana Res.* **2021**, *99*, 178–203. [CrossRef]
33. Ravindra, K.; Wauters, E.; Van Grieken, R. Variation in particulate PAHs levels and their relation with the transboundary movement of the air masses. *Sci. Total Environ.* **2008**, *396*, 100–110. [CrossRef]
34. Huang, S.; Wu, Z.; Poulain, L.; van Pinxteren, M.; Merkel, M.; Assmann, D.; Herrmann, H.; Wiedensohler, A. Source apportionment of the organic aerosol over the Atlantic Ocean from 53° N to 53° S: Significant contributions from marine emissions and long-range transport. *Atmos. Chem. Phys.* **2018**, *18*, 18043–18062. [CrossRef]
35. Barker, P.A.; Allen, G.; Flynn, M.; Riddick, S.; Pitt, J.R. Measurement of Recreational N2o Emissions from an Urban Environment in Manchester, UK. 2022. Available online: https://ssrn.com/abstract=4071514 (accessed on 2 July 2022).
36. Masella, A.P.; Bartram, A.K.; Truszkowski, J.M.; Brown, D.G.; Neufeld, J.D. PANDAseq: Paired-End assembler for illumina sequences. *BMC Bioinform.* **2012**, *13*, 31. [CrossRef]
37. Schloss, P.D.; Westcott, S.L.; Ryabin, T.; Hall, J.R.; Hartmann, M.; Hollister, E.B.; Lesniewski, R.A.; Oakley, B.B.; Parks, D.H.; Robinson, C.J.; et al. Introducing mothur: Open-Source, Platform-Independent, Community-Supported Software for Describing and Comparing Microbial Communities. *Appl. Environ. Microbiol.* **2009**, *75*, 7537–7541. [CrossRef]

38. Rognes, T.; Flouri, T.; Nichols, B.; Quince, C.; Mahé, F. VSEARCH: A versatile open source tool for metagenomics. *PeerJ* **2016**, *4*, e2584. [CrossRef]
39. Quast, C.; Pruesse, E.; Yilmaz, P.; Gerken, J.; Schweer, T.; Yarza, P.; Peplies, J.; Glöckner, F.O. The SILVA ribosomal RNA gene database project: Improved data processing and web-based tools. *Nucleic Acids Res.* **2012**, *41*, D590–D596. [CrossRef]
40. Westcott, S.L.; Schloss, P.D.; McMahon, K.; Watson, M.; Pollard, K. OptiClust, an Improved Method for Assigning Amplicon-Based Sequence Data to Operational Taxonomic Units. *Msphere* **2017**, *2*, e00073-17. [CrossRef]
41. Altschul, S.F.; Gish, W.; Miller, W.; Myers, E.W.; Lipman, D.J. Basic local alignment search tool. *J. Mol. Biol.* **1990**, *215*, 403–410. [CrossRef]
42. Sayers, E.W.; Agarwala, R.; Bolton, E.E.; Brister, J.R.; Canese, K.; Clark, K.; Connor, R.; Fiorini, N.; Funk, K.; Hefferon, T.; et al. Database resources of the National Center for Biotechnology Information. *Nucleic Acids Res.* **2018**, *47*, D23–D28. [CrossRef]
43. Dixon, P. VEGAN, a package of R functions for community ecology. *J. Veg. Sci.* **2003**, *14*, 927–930. [CrossRef]
44. Clarke, K.; Gorley, R. *PRIMER: Getting started with v6.*; PRIMER-E Ltd.: Plymouth, UK, 2005; Volume 931, p. 932.
45. Stein, A.F.; Draxler, R.R.; Rolph, G.D.; Stunder, B.J.B.; Cohen, M.D.; Ngan, F. NOAA's HYSPLIT Atmospheric Transport and Dispersion Modeling System. *Bull. Am. Meteorol. Soc.* **2015**, *96*, 2059–2077. [CrossRef]
46. Lai, C.C.; Cheng, A.; Liu, W.L.; Tan, C.K.; Huang, Y.T.; Chung, K.P.; Lee, M.R.; Hsueh, P.R. Infections caused by unusual Methylobacterium species. *J. Clin. Microbiol.* **2011**, *49*, 3329–3331. [CrossRef]
47. Szwetkowski, K.J.; Falkinham, J.O. *Methylobacterium* spp. as Emerging Opportunistic Premise Plumbing Pathogens. *Pathogens* **2020**, *9*, 149. [CrossRef]
48. Krzyściak, W.; Pluskwa, K.K.; Jurczak, A.; Kościelniak, D. The pathogenicity of the Streptococcus genus. *Eur. J. Clin. Microbiol. Infect. Dis.* **2013**, *32*, 1361–1376. [CrossRef]
49. Rogers, E.A.; Das, A.; Ton-That, H. Adhesion by pathogenic corynebacteria. *Adv. Exp. Med. Biol.* **2011**, *715*, 91–103. [CrossRef]
50. Idris, R.; Kuffner, M.; Bodrossy, L.; Puschenreiter, M.; Monchy, S.; Wenzel, W.W.; Sessitsch, A. Characterization of Ni-tolerant methylobacteria associated with the hyperaccumulating plant *Thlaspi goesingense* and description of *Methylobacterium goesingense* sp. nov. *Syst. Appl. Microbiol.* **2006**, *29*, 634–644. [CrossRef]
51. Photolo, M.M.; Sitole, L.; Mavumengwana, V.; Tlou, M.G. Genomic and Physiological Investigation of Heavy Metal Resistance from Plant Endophytic Methylobacterium radiotolerans MAMP 4754, Isolated from Combretum erythrophyllum. *Int. J. Environ. Res. Public Health* **2021**, *18*, 997. [CrossRef]
52. Rinke, C.; Rubino, F.; Messer, L.F.; Youssef, N.; Parks, D.H.; Chuvochina, M.; Brown, M.; Jeffries, T.; Tyson, G.W.; Seymour, J.R.; et al. A phylogenomic and ecological analysis of the globally abundant Marine Group II archaea (*Ca.* Poseidoniales ord. nov.). *ISME J.* **2019**, *13*, 663–675. [CrossRef]
53. Dupont, C.L.; Rusch, D.B.; Yooseph, S.; Lombardo, M.-J.; Richter, R.A.; Valas, R.; Novotny, M.; Yee-Greenbaum, J.; Selengut, J.D.; Haft, D.H.; et al. Genomic insights to SAR86, an abundant and uncultivated marine bacterial lineage. *ISME J.* **2012**, *6*, 1186–1199. [CrossRef] [PubMed]
54. Sharma Ghimire, P.; Joshi, D.R.; Tripathee, L.; Chen, P.; Sajjad, W.; Kang, S. Seasonal taxonomic composition of microbial communal shaping the bioaerosols milieu of the urban city of Lanzhou. *Arch. Microbiol.* **2022**, *204*, 222. [CrossRef] [PubMed]
55. Núñez, A.; Amo de Paz, G.; Rastrojo, A.; Ferencova, Z.; Gutiérrez-Bustillo, A.M.; Alcamí, A.; Moreno, D.A.; Guantes, R. Temporal patterns of variability for prokaryotic and eukaryotic diversity in the urban air of Madrid (Spain). *Atmos. Environ.* **2019**, *217*, 116972. [CrossRef]
56. Li, H.; Zhou, X.-Y.; Yang, X.-R.; Zhu, Y.-G.; Hong, Y.-W.; Su, J.-Q. Spatial and seasonal variation of the airborne microbiome in a rapidly developing city of China. *Sci. Total Environ.* **2019**, *665*, 61–68. [CrossRef]
57. Tanaka, D.; Fujiyoshi, S.; Maruyama, F.; Goto, M.; Koyama, S.; Kanatani, J.-i.; Isobe, J.; Watahiki, M.; Sakatoku, A.; Kagaya, S.; et al. Size resolved characteristics of urban and suburban bacterial bioaerosols in Japan as assessed by 16S rRNA amplicon sequencing. *Sci. Rep.* **2020**, *10*, 12406. [CrossRef]
58. Woo, C.; An, C.; Xu, S.; Yi, S.-M.; Yamamoto, N. Taxonomic diversity of fungi deposited from the atmosphere. *ISME J.* **2018**, *12*, 2051–2060. [CrossRef]